Short Note

Optical characterizations and reverse-bias electroluminescence observation for reliability investigations of the InGaN light emitting diode

Hsiang Chen [a,*], Yih-Min Yeh [b], Chuan Hao Liao [a], Chun Wei Lin [a], Chuan-Haur Kao [c], Tien-Chang Lu [d]

[a] National Chi Nan University, No.1, University Road, Puli, Taiwan, ROC
[b] Wu Feng University, Taiwan, ROC
[c] Chang Gung University, KueiShan, Taiwan, ROC
[d] National Chiao Tung University, Taiwan, ROC

ARTICLE INFO

ABSTRACT

The reverse-bias operation of the InGaN light-emitting diode (LED) device can reveal device-reliability problems. This study uses optical characterization techniques, including surface temperature measurements, two-dimensional (2D) X-ray fluorescent (XRF) element analysis, 2D electroluminescence (EL) images processed by Matlab, and electrical measurements to visualize the current leakages around the metal contact of the device. Connections between the device performance and the reverse-bias EL current distribution have been established. This paper attributes the origin of the reverse-bias emission to a high electric field caused by weak structures during process variations. Hot electron-induced emissions due to a leakage current may be a mechanism of the reverse-bias emission. Furthermore, reverse-bias stress on the devices is performed on the LED devices to investigate reliability issues. The reverse-bias light emission is relevant to reliability problems because of its combination of optical characterization and electrical performance. These techniques provide a screening tool that will correlate device failures with the fabrication process for future industrial applications.

1. Introduction

Researchers prefer using the InGaN/GaN light-emitting diode in the forward-bias condition, functioning as a solid-state light source. Previous research discussed the reliability issues of the LED device under reverse bias. Meneghini et al. [1] reported reverse-bias electroluminescence (EL) due to a band-to-band recombination of the stressed devices caused by leakage current flowing through preferential paths. Chen et al. investigated damage of the device induced through high reverse-bias stress by observing the reverse-bias EL [2]. In contrast to other groups, this study observes the reverse-bias electroluminescence, which was almost undetectable from the fresh device, since the luminescence behavior of the device in the reverse-bias condition could also shed light on fresh device-reliability problems. During the reverse-bias operations, field-dependent tunneling current at low voltage and local impact ionization in high-electric-field regions dominate the leakage current, which affects the device's electrical properties [3]. The goal of this study is to use optical characterization techniques, including 2D electroluminescence observation, 2D surface temperature measurements, 2D X-ray fluorescence (XRF) element analysis, and electrical measurements to explore potential

reliability problems with the InGaN LED device performance. This paper examines the EL light-emission behavior under forward-bias operations and reverse-bias operations. The reverse-bias leakage and the forward-bias subthreshold current measurements provide additional information to explore any potential reliability problems. In addition, reverse-bias stress has been performed on the LED devices. The degradation and failure caused by the reverse-bias stress further proved the possible reliability concerns with reverse-bias operations. Under a combinational study of material analysis and electrical performance, the reverse-bias electroluminescence behavior, which was a result of the hot electron-induced emission, proved relevant to the device performance. Building a nondestructive screening method could detect the current path's leakage around the metal contact and evaluate the LED device quality from the fresh device. Though the first GaN LED was demonstrated in the early 90s, the reliability problem may cloud the promise of its future development [4,5]. Therefore, numerous of studies have been conducted until now to unveil the GaN LED reliability issue. In LED industry, stress test around 6000 h is required [6,7]. This study provides fast screening techniques and locating the weakness promising for future LED industrial applications. In contrast to current industrial reliability test techniques, reverse-bias electrical analysis and reverse-bias luminescence evaluation have been conducted to exam the device reliability [8]. Understanding the mechanism and locating the weak or defect area

* Corresponding author. Tel.: +886 49 2910960x4909; fax: +886 49 2912238.
  E-mail address: hchen@ncnu.edu.tw (H. Chen).

can help engineers can improve the fabrication process and increase the yield rate [9].

2. Device fabrication

This experiment uses metal–organic chemical–vapor deposition (MOCVD) on a c-face 2 inch sapphire (0 0 0 1) substrate to grow the InGaN/GaN multiple quantum well (MQW) LED. The device structure consists of a 30 nm GaN nucleation layer, a 2-m-thick undoped GaN, 2-m-thick Si-doped n-type GaN, 100-nm-thick active layers, 50-nm-thick Mg-doped AlGaN electron-blocking layer, and a 15-nm-thick Mg-doped p-GaN layer. The InGaN/GaN MQW active region consists of 10 pairs of 3-nm-thick InGaN well layers and 7-nm-thick GaN barrier layers. After partially etching the sample down to the $n+$ layer, we deposited a 230 nm indium-tin oxide (ITO) surface layer onto the sample surface to function as the transparent contact layer (TCL). Ti/Al/Ti/Au contact was evaporated onto the exposed n-type GaN layer to function as the n-type electrode.

3. Experiments and discussion

To examine the device operations, this study investigates the electroluminescence behavior in both the forward bias and the reverse bias condition. It is common knowledge that band-to-band recombination is responsible for the forward-bias EL during the LED device operations, while band-to-band recombination [1], hot-electron emission [10,11], or yellow luminescence defect [12] and its influence on device reliability [13] may generate the reverse-bias electron emission. Not only is the reverse-bias leakage current smaller than the forward-bias recombination current, but also forward-bias band-to-band recombination contributes to strong EL. The device in the forward-bias condition generates a much stronger band-to-band recombination light emission than the leakage-current-induced emission during reverse-bias operations. The intensity of forward-bias emission is more than one million times brighter than the reverse-bias emission. In comparison to the forward-bias EL emission, the reverse-bias light emission is nearly undetectable. This study incorporates a high-resolution cooled iXON electron-multiplying charge-coupled-device (EMCCD) camera in the experiment to collect the weak light from the device under reverse-bias operations.

This study measures the surface temperature from the device under forward bias and reverse bias to associate the reverse-bias emission with the leakage current. Fig. 1(a) shows that in the forward-bias condition, high-temperature area occurs on the chip area, since current due to band-to-band recombination is flowing. The higher the current and the more power dissipation results in a higher temperature [14]. On the contrary, in the reverse-bias

condition, the temperature of the border area between the metal and the chip is higher than the chip area (Fig. 1(b)), indicating that the leakage current, which associates with the reverse-bias EL, heats up the electrode. Due to high electric field ($V = -10$ V) under reverse bias, the temperature of the border area in the reverse-bias condition is higher than the temperature of the chip area in the forward-bias condition.

To find composition of the device, this study incorporates 2D XRF element analysis to position the 2D distribution of different composite elements. XRF is a powerful tool to detect the distribution of the elements on the periodic table between Na (atomic number 11) and U (atomic number 92). Especially for some packed LED devices with resin coating or white-light LED devices with a phosphorus layer, a XRF scan can penetrate the resin coating or phosphor layer, since the XRF scan depth is approximately 5 mm for nonmetal materials, but 50 μm for metal. Using XRF analysis can clearly identify the edge of the metal contact, or the border between the chip area and the metal contact. To analyze the reverse-bias emission area, comparison of the forward-bias emission, reverse-bias emission, and element-analysis images in superposition images are investigated. Comparison of forward-bias EL and Ga XRF distribution areas (the chip area) and comparison of reverse-bias EL and Au XRF distribution areas (the metal contact) in the LED device in two superposition images are presented in Fig. 2(a) and (b). While the forward-bias emission area covers the Gallium rich area except for the near-contact area in Fig. 2(a), the reverse-bias emission occurs in the metal contact and the chip-overlapped area. Also, the line-like reverse-bias emission occurs in the square edge of circumference, which is also in the central metal area as shown in Fig. 2(b).

Although the charge-coupled device (CCD) EL image cannot reveal the metal area, the XRF analysis in Fig. 2(a) and (b) clearly presents the compositions of different parts of the device. The images demonstrate the distribution of the gold in the two electrode areas and the area surrounding the square LED chip. In addition, gallium is complementary to the two gold electrodes in the LED chip and the border between the two elements (the chip area and the electrode area) is easily identifiable. By comparing the EL images, surface-temperature profile and XRF element distribution, a reverse-bias emission emits from the border, or the contact of the central chip area where high electric field may occur due to weak structures or structural defects [15–19]. This area is vulnerable to metal migration [7,20] at the border of metal contact. The weak structure or the structural defects may be a result of process variation since the reverse-bias electroluminescence behavior differs among several devices.

This study also finds that different reverse-bias emission characteristics relates to device electrical reliability and forward-bias emission efficiency. The reverse-bias light-emission behavior
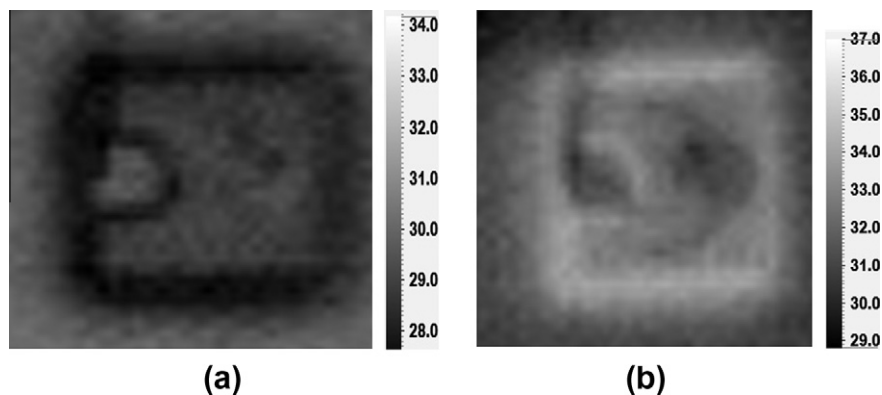
Fig. 1. Surface-temperature measurement of (a) an InGaN LED under forward bias and (b) an InGaN LED under reverse bias.
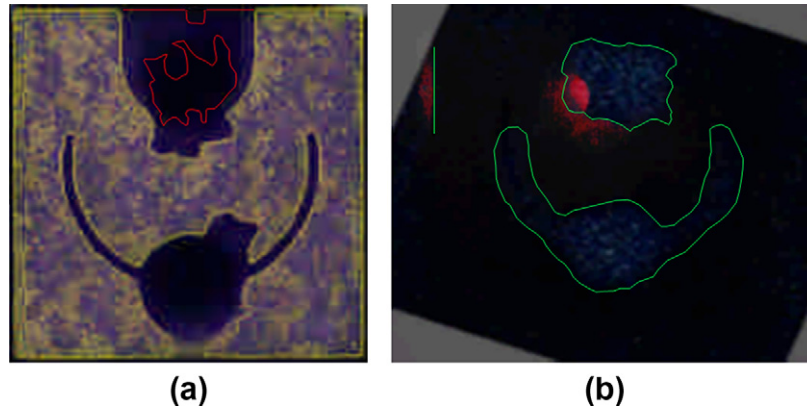
Fig. 2. (a) Comparison of forward-bias EL (in yellow), XRF Ga distribution (in purple) areas in the superposition image, and Ga distribution borderline (in red), (b) comparison of reverse bias EL (in red), XRF Au distribution (in blue) areas in the superposition image, and Au distribution borderline (in green). (For interpretation of the references to colour in this figure legend, the reader is referred to the web version of this article.)

differs among several fresh devices. At the same reverse-bias voltage of −10 V, the leakage current of the device with the largest reverse-bias emission area as shown in Fig. 3(a) (Device A) is about 100 µA and the leakage current of the device with no light emission (Device C) as shown in Fig. 3(c) has the leakage current of 5 nA. The leakage current of Device B with a small emission area, as shown in Fig. 3(b), shows the leakage current of Device B is approximately 10 µA. Most of the fresh LEDs are similar to Device C and have no reverse-bias emission.

To build connections between the device performance and the reverse-bias emission characteristics, HP 4145 measures the I–V curves of the devices with different light-emission characteristics. Fig. 4 (a), (b), and (c) show the I–V curves, which are the enlarged I–V curves under reverse bias as shown in Fig. 4(b), and the enlarged I–V curves in the subthreshold region under forward bias as shown in Fig. 4(c). In the reverse-bias condition, while Device A with the strongest reverse-bias light emission has the largest reverse-bias leakage current of approximate 100 µA order, Device C with no light emission has the smallest reverse-bias leakage current about nA order and Device C with weak light emission has the intermediate leakage current of about 10 µA order as shown in Fig. 4(b). The leakage current induces the reverse-bias emission. The larger the leakage current is, the stronger the light emission will be. We operate the LED under forward bias functioning as a light source, and we zoom into the electrical behavior of the device in the off state, subthreshold region, and fully turned-on state for the for-
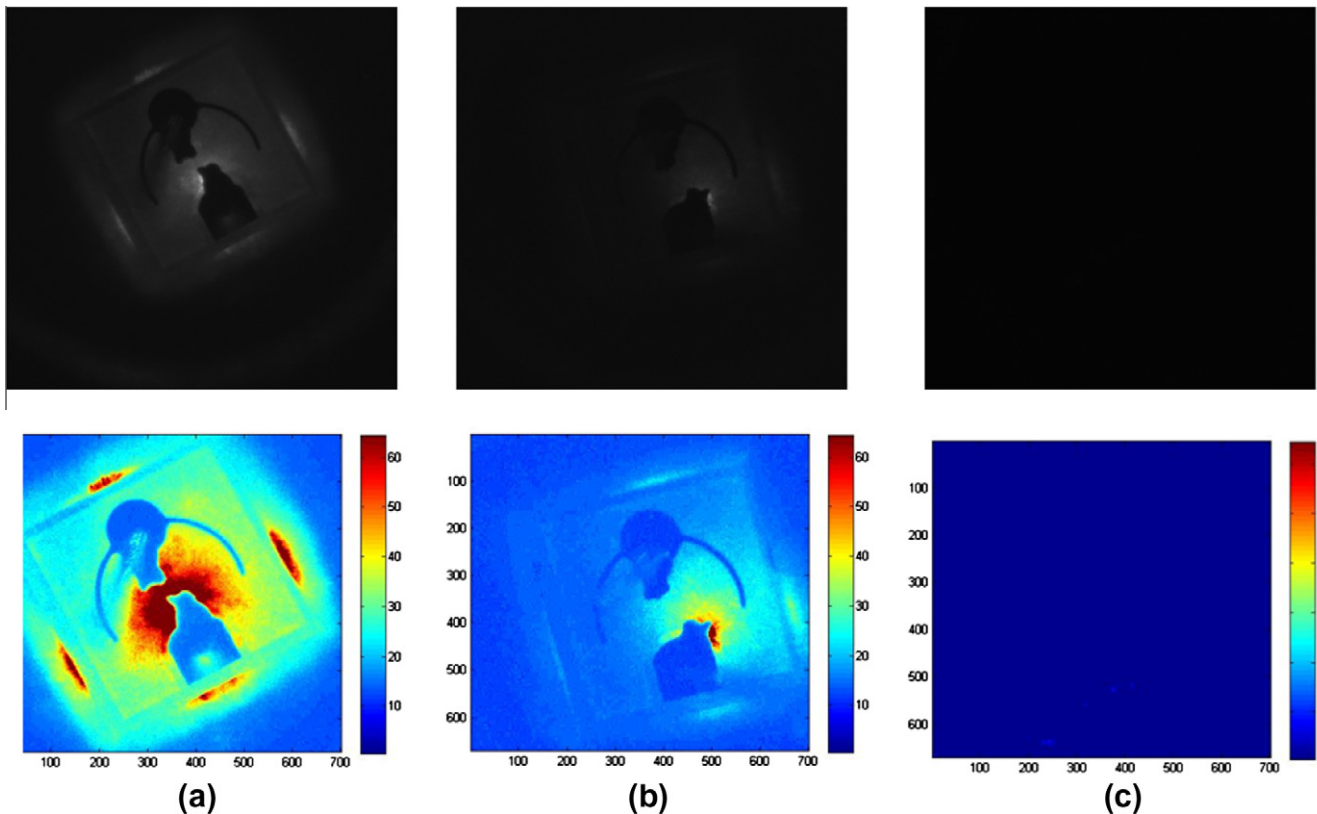
Fig. 3. The 2D Matlab processed image of (a) Device A, (b) Device B, and (c) Device C.
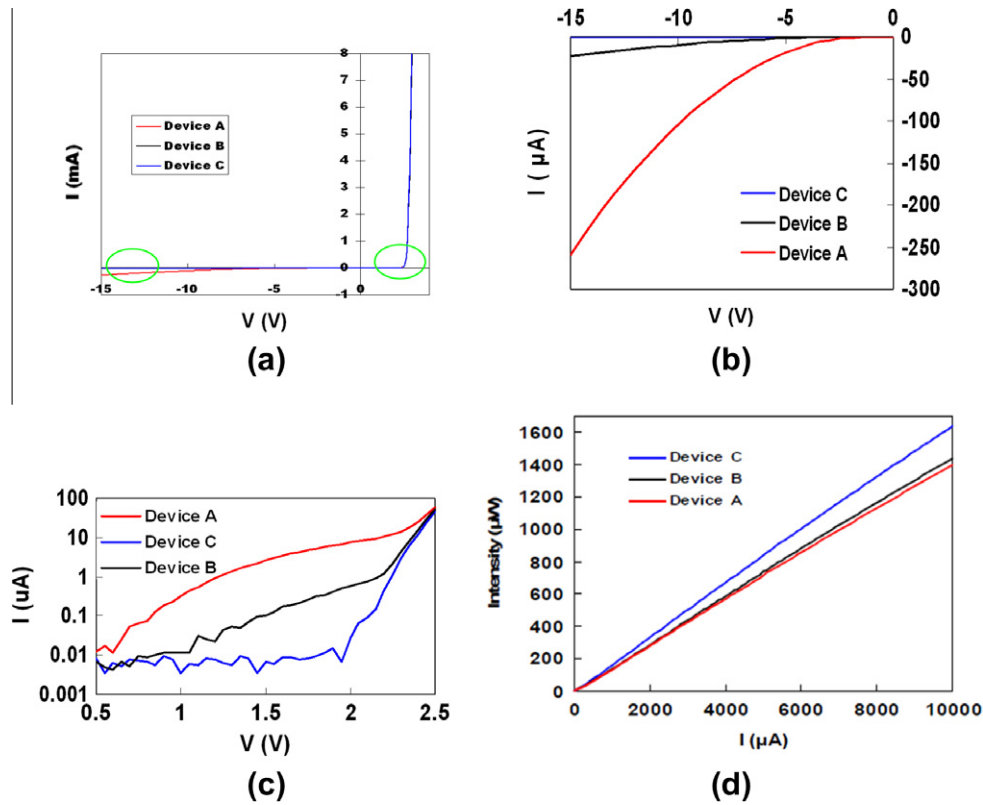
Fig. 4. (a) The I–V curves of Device A, Device B, and Device C, (b) the enlarged view of the I–V curves under reverse bias. (c) The enlarged view of the I–V curves in the subthreshold region under forward bias. (d) The L–I curves of Device A, Device B, and Device C under forward-bias.

ward-bias condition. When the three devices are in the off state and the applied voltage is below 0.5 V, the currents of the three devices are almost identical. As the applied voltage increases to 1.5 V in the subthreshold region, Device A's subthreshold current is approximately 500 times that of Device B and 50,000 times the intensity of Device C, implying that the leakage current of the devices is still present though not detectable by EL emission. The results correspond to the leakage current that relates to structure defects under forward bias and reverse bias reported by Cao et al. [18]. As the applied voltage further increases to 2.5 V in the fully turned-on region, the currents among three devices become similar again, since the strong band-to-band recombination current is so large that it has masked the leakage current. The leakage current still exists and may deteriorate the device during long-term operations.

To correlate LED forward-bias emission efficiency with the reverse-bias EL, this study evaluates the efficiency of the forward-bias light emission of these three different devices by measuring the L–I curves (Fig. 4(d)). Of the three devices, device A has the largest leakage current and the strongest reverse-bias EL but it has the lowest light-emission efficiency. The performance of device B is average. These measurements indicate that a stronger reverse-bias EL, due to the leakage-current-induced emission, results in lower device performance. In addition, this paper examines the forward-bias emission spectra of the three devices. The spectra of the three blue-light LEDs that range from 420 to 510 nm do not make a significant difference among the three devices. This implies that the reverse-bias EL of the device only relates to a decrease in emission efficiency and is irrelevant to the spectrum. Based on the reverse-bias emission characteristics, electrical prosperities, and forward-bias emission efficiency, a comparison table of the three devices is shown in Table 1.

Table 1
A comparison table of reverse-bias emission characteristics, electrical prosperities, and forward-bias emission efficiency among the three devices.

	Device A	Device B	Device C
Leakage current	100 µA	10.1 µA	5.7 nA
Normalized total intensity	1	28.5%	<0.1%
Normalized max intensity	1	52%	<1%
Normalized emission area	1	7.4%	∼0
Normalized ext efficiency	86.1%	87.7%	1

The following explains and clarifies the different mechanisms of the reverse-bias emission between the fresh device and the stressed device. The reverse-bias EL region may relate to leakage current crowding center due to a weak structure or structural defects that do not contribute to band-to-band recombination. Initially, the leakage current only induces hot electron-induced emission in the fresh device, but may have the potential to extend through a preferential path. Meneghini et al. [1,13,21] observed that the leakage current may then flow through an active region and cause yellow luminescence or band-to-band recombination from the device. Since the reverse-bias emission comes from hot electron-induced emission, the edge with emission is vulnerable to hot electron-induced emission degradation (HCID). As a result, a combination of XRF analysis and reverse-bias EL observation can help to screen the device quality. When receiving fresh LED devices, especially for devices with unknown information on their fabrication process, we can apply XRF to identify the edge or the border of the metal. Then, we use the reverse-bias EL test to identify the location of noticeable leakage current from the edge or the border of the metal and the chip area and assess the device quality just like plumbers use soapy water to find the location of the gas leak from the gas pipes.

4. Conclusion

This study investigates the mechanisms of the fresh InGaN LED device and the relationship between its performance and the reverse-bias EL with optical characterization techniques. This paper attributes the origin of the reverse-bias luminescence from the fresh device to hot electron-induced emission. As for reliability investigations of the fresh LED, we prove that the emission under reverse bias is relevant to large leakage current in the forward-bias condition, the reverse-bias condition, and low luminescence efficiency. These techniques promise a screening tool to correlate the device failures with the fabrication process.

Acknowledgments

Appendix A. Supplementary data

Supplementary data associated with this article can be found, in the online version, at http://dx.doi.org/10.1016/j.mee.2012.08.017.

References

[1] M. Meneghini, N. Trivellin, M. Pavesi, M. Manfredi, U. Zehnder, B. Hahn, G. Meneghesso, E. Zanoni, Appl. Phys. Lett. 95 (2009) 173507.

[2] N.C. Chen, Y.N. Wang, Y.S. Wang, W.C. Lien, Y.C. Chen, J. Cryst. Growth 311 (2009) 994.
[3] N. Kovalev, F.I. Manyakhin, V.E. Kudryashov, A.N. Turkin, A.E. Yunovich, Semiconductors 32 (1998) 54.
[4] M. Fukuda, Microelectron. Reliab. 40 (2000) 27.
[5] M.R. Krames, O.B. Shchekin, R. Mueller-Mach, G.O. Mueller, L. Zhou, G. Harbers, M.G. Craford, J. Disp. Technol. 3 (2007) 160.
[6] Y. Gu, N. Narendran, A non-contact method for determining junction temperature of phosphor-converted white LEDs, SPIE, 2004, pp. 107–114.
[7] H. Kim, H. Yang, C. Huh, S.W. Kim, S.J. Park, H. Hwang, Electron. Lett. 36 (2000) 908.
[8] M. Meneghini, N. Trivellin, R. Butendeich, U. Zehnder, B. Hahn, G. Meneghesso, E. Zanoni, Solidi Status C 7 (2010) 2208.
[9] D.L. Barton, M. Osinski, P. Perlin, P.G. Eliseev, J. Leeb, Microelectron. Reliab. 39 (1999) 1219–1227.
[10] H. Chen, Exploration of the Potential Defects in GaN HEMTs with Hyperspectrum Techniques, Verlag Dr. Müller, Saarbrücken, Germany, 2009.
[11] K.K. Leung, W.K. Fong, P.K.L. Chan, C. Surya, J. Appl. Phys. 107 (2010) 073103.
[12] J. Kikawa, S. Yoshida, Y. Itoh, Solid-State Electron. 47 (2003) 523.
[13] M. Meneghini, S. Vaccari, N. Trivellin, IEEE Trans. Electron Devices 59 (2012) 1416.
[14] H. Chen, P. Preecha, Z. Lai, G.P. Li, J. Electrochem. Soc. Electrochem. Soc. 159 (2008) 648.
[15] T. Honda, N. Sakai, S. Komiyama, M. Hayashi, T. Igaki, Phys. Status Solidi 9 (2012) 778.
[16] H.C. Chen, M.J. Chen, Y.H. Huang, W.C. Sun, W.C. Li, J.R. Yang, H. Kuan, M. Shiojiri, IEEE Trans. Electron Devices 58 (2011) 3970.
[17] X. Chen, A.M.C. Ng, F. Fang, Y.H. Ng, J. Appl. Phys. 110 (2011) 094513.
[18] X.A. Cao, J.A. Teetsova, F. Shahedipour-Sandvikb, S.D. Arthura, J. Cryst. Growth 264 (2004) 172.
[19] Y. Sun, T. Yu, H. Zhao, X. Shan, X. Zhang, Z. Chen, X. Kang, D. Yu, G. Zhang, J. Appl. Phys. 106 (2009) 013101.
[20] C.Y. Hsu, W.H. Lan, Y.S. Wu, Appl. Phys. Lett. 83 (2003) 2447.
[21] D. Saguatti, L. Bidinelli, G. Verzellesi, M. Meneghini, G. Meneghesso, E. Zanoni, R. Butendeich, B. Hahn, IEEE Trans. Electron Devices 59 (2012) 1402.